ESTIMATION OF LAND SURFACE TEMPERATURE AND ITS LAPSE RATE IN THE BEAS RIVER BASIN USING LANDSAT 8 DATA

Gopinadh Rongali[1*], Ashok K. Keshari[2], A. K. Gosain[2], R. Khosa[2]
1PhD Research Scholar, Department of Civil Engineering, Indian Institute of Technology Delhi, India
Email: gopinadh01@gmail.com
2Professor, Department of Civil Engineering, Indian Institute of Technology Delhi, India
Email: akeshari@civil.iitd.ac.in, gosain@civil.iitd.ac.in, rkhosa@civil.iitd.ac.in

KEYWORDS: split window, ASTER, DEM, MODIS, Himalayan

ABSTRACT
Temperature lapse rate (TLR), an essential parameter for snowmelt runoff analysis, was determined for the Beas river basin in the western Himalayas. LANDSAT 8 is formerly the landsat data continuity mission (LDCM) data was used to estimate the land surface temperature (LST) of the Beas river basin using the split window (SW) algorithm. The LST was correlated with the elevation values obtained from advanced space borne thermal emission and reflection radiometer (ASTER) and digital elevation model (DEM) data of united states geological survey (USGS) of the study area and the trend shows between LST and elevation is inverse relationship. The TLRs for the Beas area for the time period 18 April 2013 to 27 June 2015 was in the range 0.71– 0.87°C/100 m. The results was compared with lapse rates estimated using moderate resolution imaging spectroradiometer (MODIS) LST maps. TLR estimation in earlier was based on air temperature data available in meteorological stations that are sparsely located in the Himalayas. These measurements were point data and measured manually, they may have led to inaccurate results. Satellite data provides continuous and potentially unbiased recording provided an accurate radiometric calibration and atmospheric correction can be achieved. The earlier TLR estimation using air temperature from meteorological stations for the western Himalayan area was found to be 0.65°C/100 m. Air temperature and LST from LANDSAT 8 and MODIS-Terra data was found to be in good agreement and this type of studies will be useful for snowmelt runoff modelling in the Himalayan area.

1. INTRODUCTION

LST is an important factor in snowmelt runoff studies. It is defined as the surface skin temperature of the ground surface. Several efforts have been made to recover this information from satellite data. These techniques are based on an SW algorithm developed to estimate LST from LANDSAT 8 satellite was developed with the collaboration between the national aeronautics and space administration (NASA) and the USGS. The satellite was called the LDCM. The LANDSAT 8 satellite has two sensors one is operational land imager (OLI) and the second one is the thermal infrared sensor (TIRS) was successfully launched on 2013.

A number of studies have been attended to estimate LST using TIR radiation emitted from surfaces using an SW algorithm (Sobrino and Raissouni 2000; Jain et al. 2008; Jiang 2013; Tang and Li 2014; Rajeshwari and Mani 2014; Sattari and Hashim 2014; Jiménez-muñoz et al. 2014). The SW algorithm uses two adjacent TIR channels, centred at 11 mm and 12 mm, for the LANDSAT 8 to retrieve surface temperatures because of their different atmospheric transmittances. The SW LST method modifies the atmospheric effects based on the differential absorption in the infrared bands. The accuracy of the SW algorithm depends on the magnitude of the difference between the emissivities of the surface in the two bands (Becker 1987; Ruescas et al. 2016).

In this paper, an attempt was made to estimate the TLR from the LST. The SW method formulated by (Sobrino et al. 1996) for LST estimation from LANDSAT 8 data was used. This algorithm does consider emissivity values. In particular, as most of the study area is covered by snow, a uniform emissivity can be used. Hence the (Sobrino et al. 1996) algorithm was preferred over others. MODIS-Terra LST maps for the corresponding dates were used to validate the results obtained from LANDSAT 8 LST maps.

2. THE STUDY AREA AND DATA USED

For carrying out this work, the Beas river basin up to Pandoh dam has been selected as the study area (Figure 1).The Beas river basin lies in between 31º N to 32º N latitude and 77º E to 78º E longitude. The Beas river is

one of the main rivers of the Indus river system. It starts from the Rothang pass at an elevation of 3900 m and flows near north-south direction up to Larji. At Larji, it takes a right angle and turns towards the south-west and flows in the same direction up to Pandoh dam. The length of the Beas river up to Pandoh is 116 km. Among its tributaries, Parbati and Sainj Khad rivers are glacier fed. The Beas river catchment up to Pandoh dam is 5383 km^2. The catchment area mostly contains impulsive slopes and the rocks are commonly bare. There are high peaks in the east as well as in the north of the river valley. The altitude varies from 857 m near Pandoh dam up to 6582 m on the northeast border of the Parbati sub-catchment.

The primary data sets used include:

(a) LANDSAT 8 images of the study area, acquired from the USGS earth explorer data centre website. The times of satellite passes were between 10:00 am and 10:25 am local time. Six daytime images were acquired on 18 April, 5 June 2013, 21 April, 8 June 2014 and 24 April, 27 June 2015.

(b) A DEM of the study area at 30 m spatial resolution, extracted from the ASTER GDEM for Beas, which was downloaded from the USGS earth explorer data centre website.

(c) MODIS-Terra LST maps (MOD11A1) for the corresponding dates, acquired from the national snow and ice data centre (NSIDC) site.

(d) Air temperature data was downloaded from the national remote sensing centre (NRSC) from three ground stations (Chelsea, GB Pant Inst.Mohal-Kullu, and Bajaura) located within the Beas river basin (Figure 1).

The details of the data used in the study are given in Table 1.

3. METHODOLOGY

3.1 Database Creation

Using the Beas river basin tile (Tile No. 0N31E077) of the global USGS DEM, the DEM of the study area was extracted. MODIS LST and emissivity (LST/E) products provide per-pixel temperature and emissivity values. Band 26 detects cirrus clouds and TIR bands 20, 22, 23, 29 and 31–33 correct atmospheric effects and retrieve surface emissivity and temperature. The MODIS daily LST product has 12 layers, and of these, only the layer MODIS_LST_Day_1km was used in this study. The original MODIS LST data are provided in the hierarchical data format (HDF-EOS). HDF is a multi-object file format for sharing scientific data in multi-platform distributed environments. This HDF-EOS format image was exported to the '.img' format using ERDAS IMAGINE software. MODIS data version 5 uses a sinusoidal projection. This sinusoidal projection is re-projected to geographic lat/long and WGS84 data. Later the MODIS LST images were geo-referenced with the USGS-DEM. All the LST images were multiplied by a scale factor of 0.02 and 273.15 subtracted to convert the temperature into degrees Celsius. Detailed information on the MODIS LST product and methods used for MODIS LST/E product creation is given in the MODIS LST products users' guide (Riggs et al. 2006).

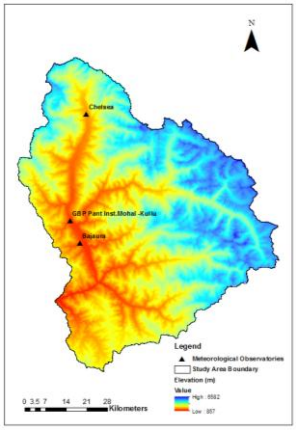

Figure 1. USGS GDEM of Beas basin up to Pandoh dam with location of meteorological observatories.

Table 1. Details of various data sets used in the present study.

Type of data	Details of data	Source of data
ASTER GDEM for Beas river basin	Spatial resolution 30 m	Downloaded from the USGS https://earthexplorer.usgs.gov/
LANDSAT 8 images	Images obtained on 18 April to 27 June 2015 with resolution of 30 m	Downloaded from the USGS https://earthexplorer.usgs.gov/
MODIS LST MOD11A1	Images obtained on 18 April to 27 June 2015 with resolution of 1 km	Downloaded from the national snow and ice data centre (NSIDC) https://nsidc.org/
Air temperature data from stations Chelsea, GB Pant Inst.Mohal-Kullu and Bajaura	AWS & IMD daily average air temperature data of Beas river basin	Downloaded from the NRSC http://www.mosdac.gov.in/

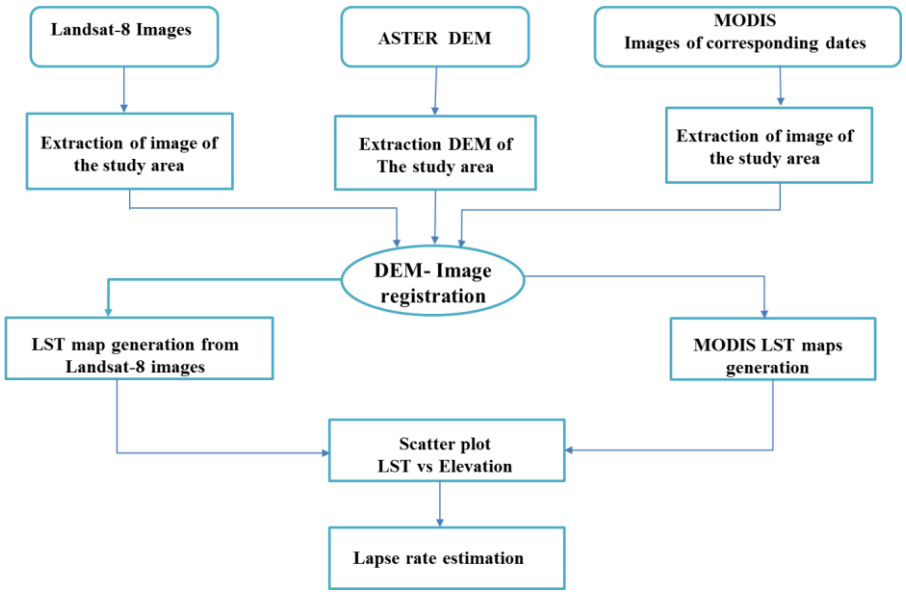

Figure 2. Flowchart illustrating the different steps involved in the LST map preparation and lapse rate determination from LANDSAT 8 thermal infrared data and ASTER DEM.

3.2 Assessment of LST

In the present study, the SW algorithm proposed by (Sobrino et al. 1996) was used to generate LST maps for the six selected LANDSAT 8 images. LST was calculated by applying a structured mathematical SW algorithm. It uses TB of two bands of TIR, mean and difference in land surface emissivity (LSE) for estimating LST of an area. The equation is:

$$LST = TB_{10} + C_1(TB_{10} - TB_{11}) + C_2(TB_{10} - TB_{11})^2 + C_0 + (C_3 + C_4 W)(1 - m) + (C_5 + C_6 W)\Delta m \quad (1)$$

Where,

LST = Land surface temperature (K)

C_0 to C_6 = Split window coefficient values (Table 2) (Skokovic et al. 2014; Sobrino et al. 1996; Zhao et al. 2009)

TB_{10} and TB_{11} = Brightness temperature of band10 and band11 (K)

m = mean LSE of TIR bands

W = Atmospheric water vapor content

Δm = Difference in LSE

Table 2. SW Coefficient values

Constant	Value
C_0	-0.268
C_1	1.378
C_2	0.183
C_3	54.300
C_4	-2.238
C_5	-129.200
C_6	16.400

3.2.1 Top of Atmospheric Spectral Radiance

The value of the top of atmospheric (TOA) spectral radiance ($L\lambda$) was determined by multiplying multiplicative rescaling factor (0.000342) of TIR bands with its corresponding TIR band and adding additive rescaling factor (0.1) with it. Estimation of TOA spectral radiance of TIRS band 10 and 11 and OLI sensor of band 2-5 individually using the algorithm given below. This algorithm transforms the raw image into spectral radiance image. Using ARC MAP 10.3 raster calculator implements algorithm of equation 2 to perform task,

$$L\lambda = \left(\frac{L_{\max} - L_{\min}}{DN_{\max}}\right) \times Band + L_{\min} \quad (2)$$

Where,

$L\lambda$ – Top of atmospheric spectral radiance in watts/ ($m^2 \times srad \times \mu m$)

$L_{\max}$ – Maximum spectral radiance of respective band

$L_{\min}$ – Minimum spectral radiance of respective band

$DN_{\max}$ = $Qcal_{\max} - Qcal_{\min}$ = Difference of maximum and minimum calibration of sensor

3.2.2 Brightness Temperature

TB is the microwave radiation radiance traveling upward from the top of Earth's atmosphere. The calibration process has been done for converting thermal DN values of thermal bands of TIR to TB. The finding TB of an area the TOA spectral radiance of ($L\lambda$) was needed. TB for both the TIRs bands were calculated by adopting the following formula, estimation of TB of band 10 and 11. TB is the electromagnetic radiation traveling upward

from the top of the Earth's atmosphere. Thermal calibration process done by converting thermal DN values of raw thermal bands of TIR sensor into TOA spectral radiance and after using TB equation shown in equation 3.

Brightness temperature = $TB = K2/(\ln(K1/L\lambda + 1)) - 273.15$ (3)

Where,
$K1$ and $K2$ – Thermal constant of bands from metadata image file
L – Top of atmospheric spectral radiance layer

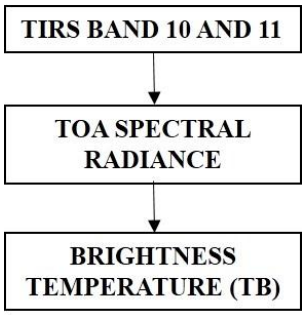

Figure 3. Flowchart of thermal calibration process

3.2.3 NDVI Threshold

OLI bands 2, 3, 4 and 5 were layer stacked and normalized difference vegetation index $(NDVI)$ was calculated using ERDAS IMAGINE software. The output value of $NDVI$ ranged between -0.26 to 0.61. To get $NDVI_s$ and $NDVI_v$, the $NDVI$ image was reclassified into soil and vegetation and the classified data were used to find out fractional vegetation cover (FVC). After generating LSE for both the bands of TIR, the mean and difference LSE was found as, estimation of $NDVI$ using OLI sensor optical band after layer stacking of band 2,3,4,5 using algorithm shown in equation 4.

$$NDVI = \frac{Band_5 - Band_4}{Band_5 + Band_4} = \frac{NIR - RED}{NIR + RED} \quad (4)$$

Range: -1< $NDVI$ <+1

3.2.4 Fractional Vegetation Cover

Estimation of FVC for an image using $NDVI$ image obtain from above step using the equation 5. FVC estimate the fraction of an area under vegetation. Figure 4 shows the flowchart to perform FVC. SW algorithm utilizes FVC to estimate LSE. Using ARC MAP 10.3 we reclassify the $NDVI$ layer into soil and vegetation and calculate $NDVI$ for soil and vegetation and implement the algorithm of FVC of equation 6.

$$FVC = \frac{NDVI - NDVI(Soil)}{NDVI(Vegetation) - NDVI(Soil)} \quad (5)$$

$$FVC = \frac{NDVI - 0.15}{0.48 - 0.15} \quad (6)$$

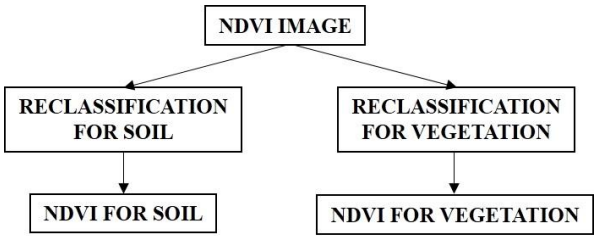

Figure 4. Flowchart for FVC

3.2.5 Land surface emissivity

To find LST it is necessary to calculate the LSE of the region. LSE was estimated using $NDVI$ threshold method. Estimation of LSE from FVC layer obtain from above step using the algorithm in equation 7. LSE measure the inherent characteristic of the earth surface. It measures its ability to convert thermal or heat energy into radiant energy. LSE estimation required emissivity of soil and vegetation of both band 10 and 11 are given in Table 3. LSE of band 10 and 11 are individually calculated.

$$LSE = \varepsilon_s \times (1 - FVC) + \varepsilon_v \times FVC \tag{7}$$

Where,

ε_s = Emissivity for soil

ε_v = Emissivity for vegetation

FVC = Fractional vegetation cover

Table 3. Emissivity values

Emissivity	Band10	Band11
ε_s	0.971	0.977
ε_v	0.987	0.989

(Source: Skokovic et al. 2014; Sobrino et al. 1996; Zhao et al. 2009)

3.2.6 Mean and Difference of LSE

Combination of LSE of band10 and LSE of band 11 obtain from above step through mean and difference in between them as shown in equation 8 and 9.

Mean of $LSE = m = \dfrac{LSE_{10} + LSE_{11}}{2}$ (8)

Difference of $LSE = \Delta m = LSE_{10} - LSE_{11}$ (9)

3.2.7 Land Surface Temperature

Estimation of LST using the algorithm in equation 10 implemented. Finally, the LST in kelvin was determined using SW algorithm.

$$LST = TB_{10} + C_1(TB_{10} - TB_{11}) + C_2(TB_{10} - TB_{11})^2 + C_0 + (C_3 + C_4 W)(1 - m) + (C_5 + C_6 W)\Delta m \tag{10}$$

Where,

TB_{10} and TB_{11} – Brightness temperature of band 10 and 11

C_0 - C_9 – Split window coefficient values

m – Mean LSE

Δm – Difference of LSE

W – Atmospheric water-vapour content

Table 4. $NDVI$ for soil and vegetation

$NDVI$ for soil	0.15
$NDVI$ for vegetation	0.48

This algorithm does consider emissivity of the surface. As the data used in this study are of 30 m spatial resolution, and most of the study area is covered by snow, it was assumed that the reflectivity of snow is uniform. Therefore, (Sobrino et al. 1996) algorithm was used for LST retrieval from LANDSAT 8 images.

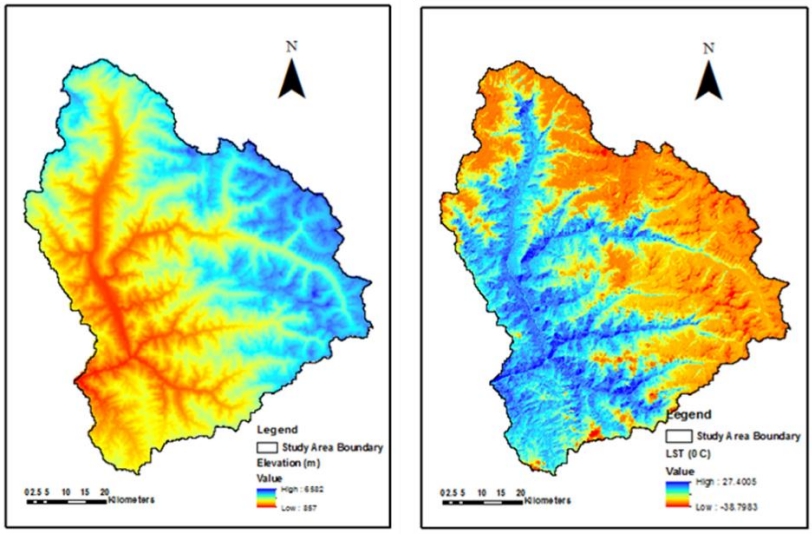

Figure 5. Visual comparison between the (a) ASTER DEM and (b) LST map derived from the LANDSAT 8 image of 24 April 2015.

A statistical analysis was carried out between DEM and the LANDSAT 8 and MODIS LST maps to determine the relationship between elevation and LST (Figure 6 and 7). Using the regression equations, the lapse rate of the study area was determined for twelve dates.

4. RESULTS AND DISCUSSION

The present study was conducted in the Himalayan region in which a number of snowmelt runoff studies have been carried out and are in progress (Gupta et al. 2005). As such no ground measurements of LST are available in the field, the LST obtained from LANDSAT 8 and MODIS data were compared with the air temperature observed at three stations.

The relationships between air temperature and LST from LANDSAT 8 and MODIS data, depicted in Figure 8 is in close agreement. In general, air temperature is higher than LST for most points. The present study clearly demonstrates a negative linear correlation between LST and elevation. A map depicting a variation of LST obtained from LANDSAT 8 data for 24 April 2015 is shown in Figure 5(b).

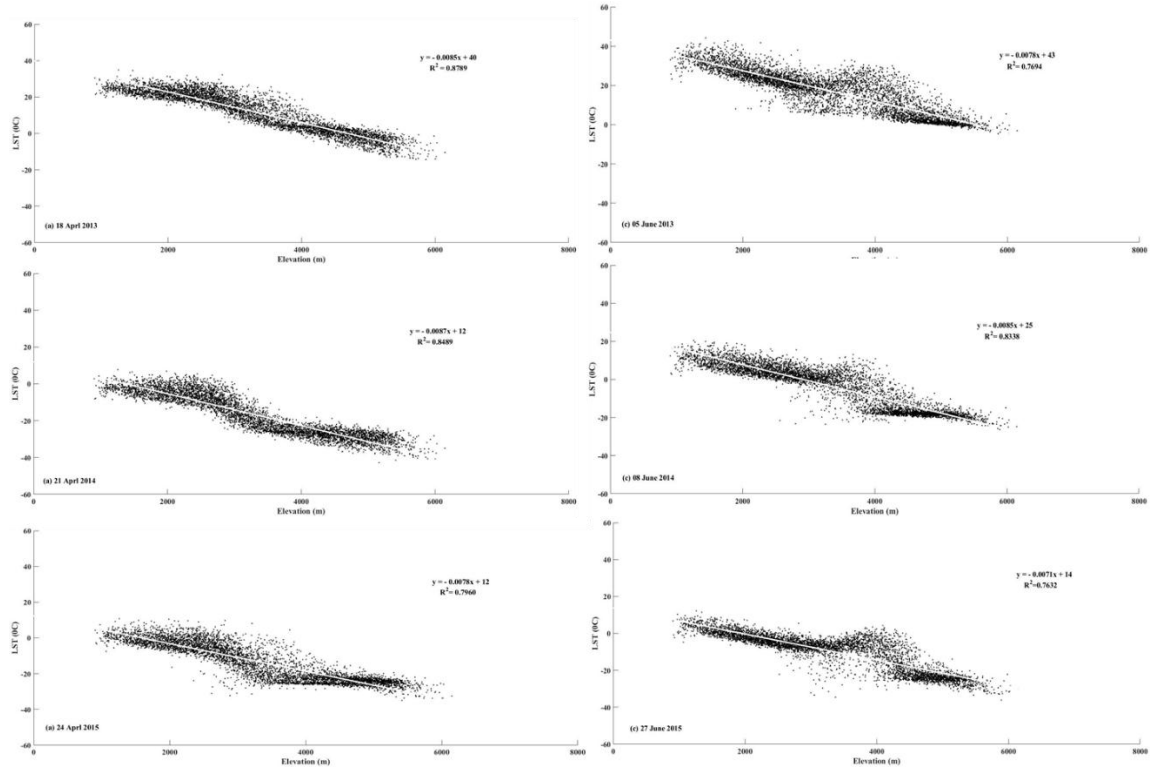

Figure 6. Scatter plots showing the temperature-elevation relationship (ASTER DEM vs. LST map derived from LANDSAT 8 images) at six different dates.

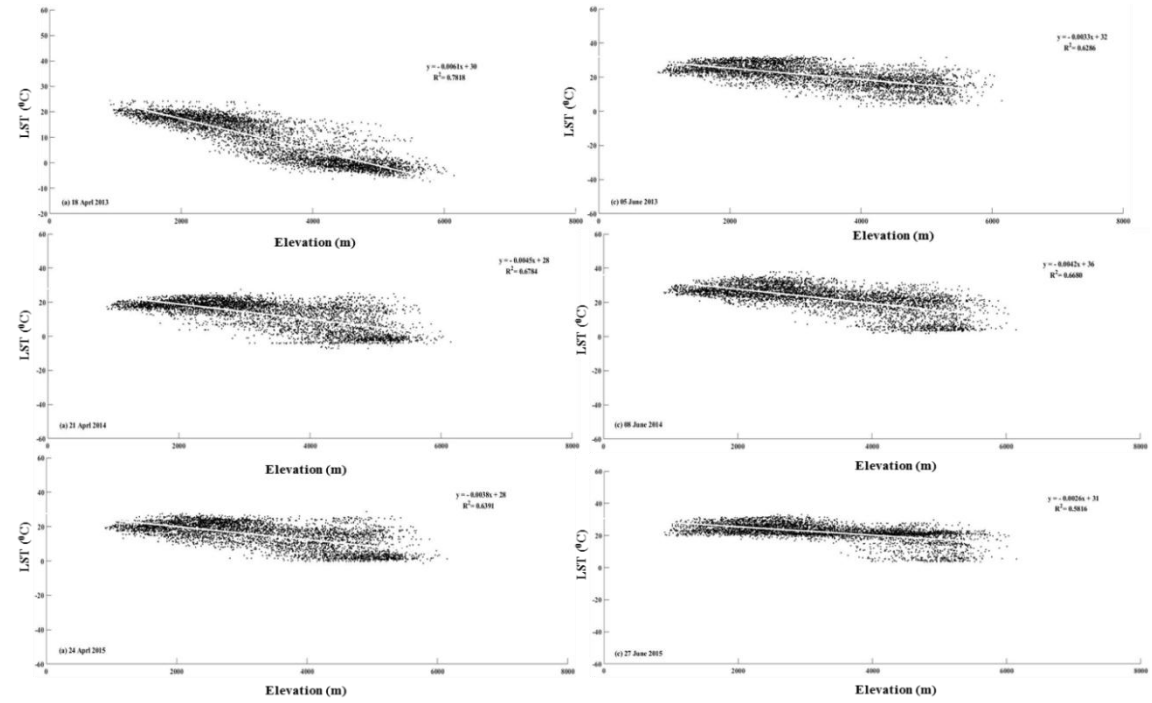

Figure 7. Scatter plots showing the temperature-elevation relationship (ASTER DEM vs. LST map derived from MODIS images) at six different dates.

A comparison of LST maps with the elevation map (Figure 5(a)) shows that the temperature follows a similar pattern as elevation. Saraf et al. (2005) have also reported a negative linear correlation between LST and elevation. They used this relationship to prepare a DEM from NOAAAVHRR night-time thermal images. Using the lapse rate values and the linear regression equations, the LSTs were estimated for different dates from LANDSAT 8 and MODIS data for the selected stations. These LST values were compared with the corresponding air temperature values, and the result is shown in Figure 8. The Figures clearly shows that the difference between LST and air temperatures is not significant.

Figures 6 and 7 show scatter plots for LST obtained from LANDSAT 8 and MODIS datasets and air temperature. These clearly show that temperature decreases with an increase in elevation in a linear manner. The equations of the regression line obtained from the plots can be generalized as follows:

$$Y = -aX + b \tag{11}$$

where X is the elevation value and Y is the temperature value. As the slope of the line ($-a$) is negative, it indicates that the temperature and LST values plotted in the scatter plots are inversely related to each other. The values of the coefficient of determination (R^2) were also computed for the scatter plots (Figures 6 and 7).

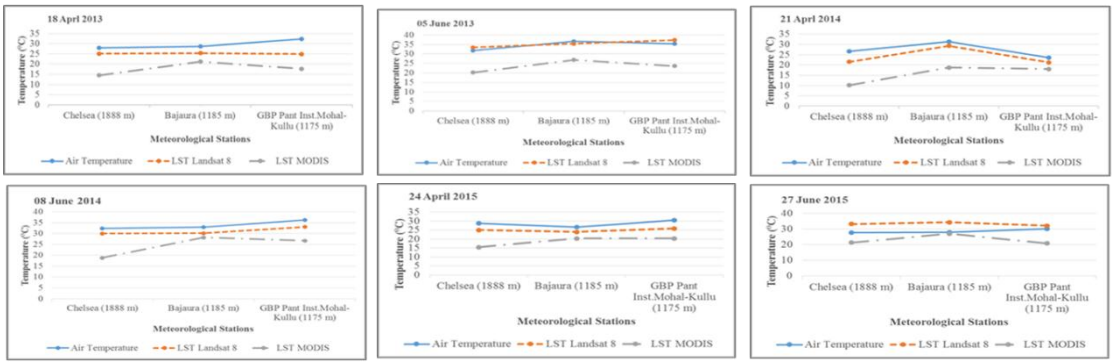

Figure 8. Comparison between air temperature data, LST values from LANDSAT 8 and LST values from MODIS for six different dates at three different stations.

R^2 represents the fraction of initial variance accounted for by the relationship and it varies between 0 and 1. If the value is zero then it indicates that the two variables are not related to each other. In the present study, R^2 values between 0.763 and 0.878 were obtained in the case of LST from LANDSAT 8 images and R^2 values between 0.581 and 0.781 in the case of MODIS LST maps, which indicates that the two variables, LST and elevation, are highly inversely correlated to each other. The LANDSAT 8 LST is better correlated with the elevation values as compared with MODIS LST data.

The slope of the equations (Figures 6 and 7) is equal to the lapse rate. The results show that TLR, estimated for the study area from LST and DEM is in the range 0.71–0.87ºC/100m for the LANDSAT 8 LST values and 0.26–0.61°C/100m for the MODIS LST values. TLR is not a constant but changes with region and season. According to (Bolstad et al. 1998), TLR estimated from air temperature data shows slightly seasonal trends and averaged 4–10ºC/km when the maximum temperature was considered. Minimum TLRs also varied with season and averaged from -3°C to 5.7ºC. As the images considered for the LST retrieval were of different dates/season, hence a difference of about 0.15°C/100m (or 1.5ºC/km) is acceptable.

5. CONCLUSIONS

In snowmelt runoff studies, air temperature is an important component. In rugged terrain such as the Himalayas, meteorological stations collecting air temperature data are sparsely located and the observations, being point data, are not representative of the whole terrain. In addition, the air temperature is measured manually and hence it is susceptible to errors. In such conditions, LST maps prepared from satellite images are an attractive alternative. LST maps provide a continuous dataset. They are prepared from satellite data, which automatically measure

radiance values, making them free from human error provided an accurate radiometric calibration of the sensor channels is achieved. In this study, LST was measured for the Beas river basin using the SW algorithm and the lapse rate of the LST was computed using elevation maps for 18 April, 5 June 2013, 21 April, 8 June 2014, 24 April, 27 June 2015. The TLR in the case of LST varied from 0.71°C/100m to 0.87ºC/100 m. The range of lapse rate obtained from the present study can be used with confidence in snowmelt runoff and other studies. This approach can also be used for estimation of seasonal variation in TLR of LST. The LANDSAT 8 images and MODIS LST maps are supplied free of charge for research purpose, which makes them economically suitable. In addition, the above-mentioned datasets are available for near real time, providing a further advantage. There is research potential for the use of LST data in snowmelt runoff computations.

ACKNOWLEDGEMENTS

We wish to thank the national remote sensing centre (NRSC), Hyderabad, India for providing the air temperature data used in this study. Thanks are also united states geological survey (USGS) earth explorer and national snow and ice data centre (NSIDC) for providing the LANDSAT 8 and MODIS satellite data with free of cost to this work.

REFERENCES

Becker F (1987) The impact of spectral emissivity on the measurement of land surface temperature from a satellite. INT J Remote Sens 8:1509–1522. doi: 10.1080/01431168708954793

Bolstad P V, Swift L, Collins F, et al (1998) Measured and predicted air temperatures at basin to regional scales in the southern Appalachian mountains. Agric For Meteorol 91:161–176. doi: 10.1016/S0168-1923(98)00076-8

Gupta RP, Haritashya UK, Singh P (2005) Mapping dry/wet snow cover in the Indian Himalayas using IRS multispectral imagery. Remote Sens Environ 97:458–469. doi: 10.1016/j.rse.2005.05.010

Jain SK, Goswami A, Saraf a. K (2008) Determination of land surface temperature and its lapse rate in the Satluj River basin using NOAA data. Int J Remote Sens 29:3091–3103. doi: 10.1080/01431160701468992

Jiang G-M (2013) Development of Split-Window Algorithm for Land Surface Temperature Estimation From theVIRR/FY-3A Measurements. 10:952–956.

Jiménez-muñoz JC, Sobrino J a, Skokovi D, et al (2014) Land Surface Temperature Retrieval Methods From Landsat-8 Thermal Infrared Sensor Data. 11:1840–1843.

Rajeshwari a, Mani ND (2014) Estimation of Land Surface Temperature of Dindigul District Using Landsat 8 Data. 122–126.

Riggs G, Hall D, Salomonson V (2006) MODIS snow products user guide to collection 5. Digit Media 6:1–80.

Ruescas A, Danne O, Fomferra N, Brockmann C (2016) The Land Surface Temperature Synergistic Processor in BEAM: A Prototype towards Sentinel-3. Data 1:18. doi: 10.3390/data1030018

Sattari F, Hashim M (2014) A Breife Review of Land Surface Temperature Retrieval Methods from Thermal Satellite Sensors. 22:757–768. doi: 10.5829/idosi.mejsr.2014.22.05.21934

Skokovic D, Sobrino JA, Jiménez Muñoz JC, et al (2014) Calibration and Validation of land surface temperature for Landsat8- TIRS sensor TIRS LANDSAT-8 CHARACTERISTICS. L Prod Valid Evol ESA/ESRIN 27.

Sobrino JA, Li Z, Stoll MP, Becker F (1996) Multi-channel and multi-angle algorithms for estimating sea and land surface temperature with ATSR data. Int J Remote Sens 17:2089–2114. doi: 10.1080/01431169608948760

Sobrino JA, Raissouni N (2000) Toward remote sensing methods for land cover dynamic monitoring: Application to Morocco. Int J Remote Sens 21:353–366. doi: 10.1080/014311600210876

Tang H, Li Z-L (2014) Land Surface Temperature Retrieval from Thermal Infrared Data. Quant Remote Sens Therm Infrared 11:1840–1843. doi: 10.1007/978-3-642-42027-6

Zhao S, Qin Q, Yang Y, et al (2009) Comparison of two split-window methods for retrieving land surface temperature from MODIS data. J Earth Syst Sci 118:345–353. doi: 10.1007/s12040-009-0027-4